Materials Science and Engineering C 32 (2012) 2390–2395

Contents lists available at SciVerse ScienceDirect

Materials Science and Engineering C

journal homepage: www.elsevier.com/locate/msec

Depth-dependent normal strain of articular cartilage under sliding load by the optimized digital image correlation technique

Chun-Qiu Zhang, Li-Lan Gao *, Li-Min Dong, Hai-Ying Liu

Tianjin Key Laboratory for Control Theory & Applications in Complicated Industry Systems, School of Mechanical Engineering, Tianjin University of Technology, Tianjin 300384, PR China

ARTICLE INFO

Article history:
Received 29 December 2011
Received in revised form 26 May 2012
Accepted 4 July 2012
Available online 11 July 2012

Keywords:
Articular cartilage
Depth-dependent
Normal strain
Friction force
Optimized DIC technique
Sliding load

ABSTRACT

The sliding experiments of articular cartilage were conducted by applying an optimized digital image correlation (DIC) technique and the depth-dependent normal strain and friction force were analyzed for cartilage. It is found that the friction forces of cartilage increase firstly and then decrease slowly with the slide of slider and increase with increasing compressive strain. The normal strain values of different layers increase obviously with sliding time with compressive strain of 35.2%. The normal strain values of superficial layer and middle layer appear in an increasing trend however little change of normal strain in deep layer is observed with sliding time with compressive strains of 18.9% and 11.2%. The depth-dependent normal strain values decrease along depth direction with constant compressive strain and the normal strain values of different normalized depth increase with increasing compressive strain. The friction forces and depth-dependent normal strain values of cartilage decrease slightly with increasing sliding rates. It is noted that the first sliding friction forces are the largest and then the friction forces decrease with increasing sliding numbers. The normal strain value increases with increasing sliding numbers and the increasing amplitude of normal strain during the former two sliding is significant. The fitting relationship of normal strain and normalized depth was obtained considering the effects of compressive strain and sliding rate and the fitting curves agree with the experimental data for cartilage with different compressive levels and sliding rates very well.

1. Introduction

Articular cartilage serves as the load-bearing and avascular tissue with excellent friction, lubrication and wear characteristics [1]. It covers the surfaces of subchondral bones in diarthrodial joints to transmit loads, absorb shock and sustain daily loading histories generating time-varying, spatial distributions of stresses and strains. The cartilage is exposed to a wide range of loads up to 10 times the body weight and is subjected to both static and dynamic loads including sliding and rolling motions in activities of daily living. So it is significant to investigate the mechanical behavior of articular cartilage under these physiological loads considering the importance of cartilage in maintaining the mobility and quality of life of individuals. In this study, the optimized digital image correlation (DIC) technique was applied to investigate the depth-dependent mechanical behavior for articular cartilage under sliding load for the first time.

Many studies have been made on the friction properties of cartilage under sliding load [2–11]. Katta et al. [7] investigated the friction properties of cartilage against cartilage at different contact stress levels under static and dynamic load conditions and it was found that the increasing contact stress reduced the friction levels. Forster and Fisher [8] found that the friction coefficients of the initial and repeat tests were both dependent on the loading time by the reciprocating friction tests of cartilage-on-metal contact. Li et al. [9] studied the friction behavior of cartilage-on-PVA hydrogel contact, cartilage-on-cartilage contact and cartilage-on-stainless steel contact under static load and cyclic load. It was concluded that the friction coefficient of cartilage-on-cartilage contact maintained far lower value than other contacts. Caligaris [10] reported that migrating contact area, which delivers re-swelling periods to the tissue, significantly promoted the sustainability of the interstitial fluid pressurization mechanism and consequent low friction coefficient. Pawaskar [11] introduced the sliding motion into a biphasic FE model and remarked the importance of migrating contact area for sustainability of the biphasic lubrication. However the effect of material structure has not been sufficiently evaluated for sliding motion.

Microscopically, articular cartilage shows inhomogeneity and anisotropy in its structure and composition. The structure of cartilage is described in three distinct zones along the depth direction: superficial, middle and deep [12–15]. In superficial zone, collagen fibrils are oriented parallel to the articular surface and concentration of proteoglycan content is lowest within three zones. In the middle zone, orientation of fibrils tends to be vertical to the articular surface and proteoglycan content increases. In the deep zone, collagen fibrils are perpendicular to the articular surface. Other properties of cartilage, such as density of collagen fibrils, water content, fixed charge density, morphology of cells, etc., vary along depth direction [16–22]. Consequently, the tissue's

* Corresponding author. Tel.: +86 22 60214133.
E-mail address: gaolilan780921@163.com (L.-L. Gao).

0928-4931/$ – see front matter © 2012 Elsevier B.V. All rights reserved.
doi:10.1016/j.msec.2012.07.012

mechanical properties vary through the depth of cartilage. Wang et al. [23] found that the depth-dependent elastic modulus and Poisson's ratio of cartilage were the smallest at the articular surface and increased with depth under unconfined compression. Gao et al. [24] investigated the depth-dependent relaxation behavior and Young's modulus under unconfined compression and it was found that the inhomogeneous relaxation modulus which is the ratio of the stress at certain relaxation time point to the depth-dependent strain increased obviously with cartilage depth and the nearly five times differences between the surface zone and deep zone were observed for different relaxation time under given strain levels. The Young's modulus increased with depth and both the magnitude and the variation of the Young's modulus were affected by increasing strain rates. Sakai [25] found that the local compressive strain varied through the depth of cartilage by compressive test. However there are few researches on depth-dependent mechanical behaviors of articular cartilage under sliding load.

In this study, the depth-dependent mechanical behavior of articular cartilage under sliding load was investigated by applying the optimized digital image correlation (DIC) technique. The depth-dependent normal strain distributions were obtained with different compressive levels and sliding rates. Simultaneously the effects of compressive level, sliding rate and sliding number on the friction force of cartilage have also been analyzed.

2. Materials and methods

2.1. Materials

Articular cartilage from the trochlea site of about 8-month-old pig knee joint was obtained 4–6 h post-mortem from a local slaughterhouse. A steel trephine was used to harvest cartilage-bone plugs with the trephine core axis perpendicular to the articular surface. Then twenty-seven full-thickness cartilage samples with subchondral bone taken from four joints were made in dimension of about 6 mm in length, 4 mm in width, 2 mm in thickness and were separated into nine groups. Before conducting the experiment all samples were soaked in saline so as to maintain the humidity of the cartilage.

2.2. Experimental apparatus

The friction test of articular cartilage under sliding load was performed on a MTF-100 testing machine (Center of Mechanical Experiment in Shanghai University, China). The machine mainly consists of image acquisition system, mechanical loading system, computer control system and image processing software. The progressive scan CCD camera is applied and the 1376×1035, 8 bit images can be obtained for the image acquisition system. The loading rate of mechanical loading system is 0.01 mm/min-100 mm/min and the load capacity is 100 N. The captured sequential images were analyzed using the image processing software to generate the displacement fields and the strain fields. Fig. 1 shows the experimental setup under sliding load.

Cartilage specimen was fixed in the center of the test chamber with saline solution as shown in Fig. 1. The cylindrical slider with 35 mm diameter and a surface roughness of Ra and 0.05 was driven by a ball screw and a servomotor and was in the horizontally reciprocating sliding state on the surface of the cartilage sample. The friction force was measured with a uniaxial load cell mounted on the translation stage and the sliding displacement of the platen was monitored by displacement sensor. The microscope was focused on the cross section of cartilage sample and all images captured contained the whole thickness of the cross section. The strain fields of cartilage sample were obtained by processing the captured sequential images.

2.3. Methods

An optimized digital image correlation technique was applied to measure the two-dimensional deformation fields in the cartilage samples under sliding load. The essence of this technique is to automatically measure displacements by tracking the change in position of points on digitized images of the object's surface. The optimized digital image correlation requires a random pattern on the sample surface that can be readily identified in sequential images. This random pattern enables us to perform digital image correlation of sequential images that record the deformation of the sample. In this study the iron oxide nanoparticles, which were scattered and embedded in the cartilage sample profile, were used as fiducial markers for cartilage sample and the relative position of these nanoparticles gave rise to a random pattern on the sample surface. Fig. 2 shows microscopic images of a section of cartilage sample before and after loading. Considering a point of interest A in the image of the reference configuration the corresponding point A′ was obtained in the image of the deformed configuration. The normal deformation (along cartilage depth direction) is observed as shown in Fig. 2 and the normal strain can be determined by the following relationship.

$$\varepsilon_Z = \left(z' - z\right)/h \tag{1}$$

Where ε_Z is the normal strain and h is the thickness of cartilage.

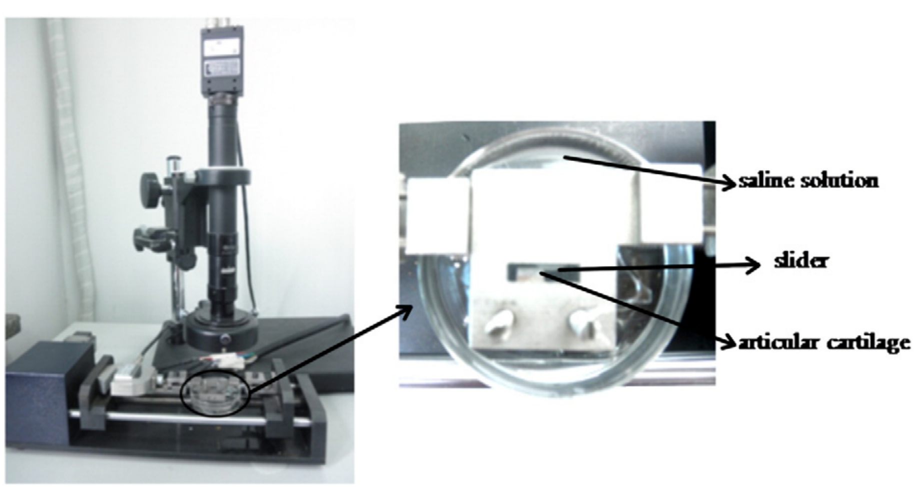

Fig. 1. Experimental setup for articular cartilage under sliding load.

2.4. Experimental description

The continuous sliding tests were conducted with given compressive strain values of 11.2, 18.9 and 35.2% and at different sliding rates of 0.33, 0.83 and 1.67 mm/s for nine sets of independent cartilage specimens respectively. The slider was reciprocated 10 times over the cartilage samples with a distance of 6 mm in each test. For each condition three samples were tested considering random error.

Prior to any sliding load the initial thickness of each sample was measured microscopically and the image of the sample in its load-free reference state was first acquired. The samples were also imaged during the whole sliding process and the images were analyzed using the optimized DIC technique to generate the displacement fields and the strain fields. The friction force and sliding displacement were measured and recorded by the testing machine.

2.5. Fitting model

Based on the experimental data of cartilage samples with different compressive strains and sliding rates the relation of the normal strain and normalized depth considering the effects of compressive strain and sliding rate was fitted as the following.

$$\varepsilon_Z = \varepsilon_1 + \varepsilon_2 \cdot \exp(aZ) \tag{2}$$

$$\varepsilon_1 = -0.4054\varepsilon_0^2 - 0.1372\varepsilon_0 - 0.0199 \tag{3}$$

$$\varepsilon_2 = 1.1184\varepsilon_0^2 + 0.8158\varepsilon_0 + 0.0463 \tag{4}$$

$$a = 0.0376V^2 - 0.2352V - 1.2143 \tag{5}$$

Where ε_Z is the normal strain, ε_0 is the applied compressive strain, ε_1 and ε_2 are the parameters related with the ε_0, a is related with the sliding rate V. Z is the normalized depth and $Z=0$ corresponds to the cartilage surface.

3. Statistical analysis

A one-way analysis of variance (ANOVA) with repeated measures was performed to detect the differences among the experimentally measured values of friction force in three sliding tests. Similarly, the ANOVA with repeated measures was applied to detect differences among the normal strain values in three sliding tests. Statistical significance was accepted for $p<0.05$. Data points shown in the figures of the next section represent mean values, whereas error bars indicate the standard errors above and below corresponding mean values.

4. Results

4.1. Effect of compressive strain value on friction force of articular cartilage

The effect of compressive strain value on friction force of articular cartilage was investigated by sliding tests and Fig. 3 shows the relationship of friction force and sliding displacement with different compressive strain values at a constant sliding rate. It is noted that the friction forces of the cartilage increase firstly and then decrease slowly with the slide of the slider and the friction forces increase with increasing compressive strain values.

4.2. Effect of compressive strain value on normal strain of articular cartilage

The normal strains of different layers for cartilage were investigated with sliding time and the effect of compressive strain value on normal strain was analyzed as shown in Fig. 4. It is found that the normal strain values of different layers increase obviously with sliding time with compressive strain of 35.2%. The normal strain values of the superficial layer and middle layer appear in an increasing trend however little change of normal strain in deep layer is observed with sliding time with compressive strain of 18.9% and 11.2%. The normal strain values of different layers for cartilage increase with increasing compressive strain.

Fig. 5 shows the distributions of normal strain through cartilage depth with different compressive strain values at sliding rate of 0.33 mm/s in order to display the effect of compressive strain on depth-dependent normal strain of cartilage more clearly. It is shown that the normal strain value decreases along the cartilage depth with constant compressive strain. The normal strain values of different normalized depth for cartilage increase with increasing compressive strain and the increasing amplitude of normal strain is the largest in the superficial layer. The distributions of normal strain through cartilage depth with different compressive strains were fitted by the expressions (2), (3), (4) and (5) and the fitting curves agree with the experimental data very well as shown in the Fig. 5.

4.3. Effect of sliding rate on friction force and normal strain of articular cartilage

The effect of sliding rate on friction force and normal strain of articular cartilage was investigated by sliding tests and Fig. 6 shows the relationship of friction force and sliding displacement at different sliding rates with constant compressive strain value. It is noted that the friction forces of cartilage decrease slightly with increasing sliding

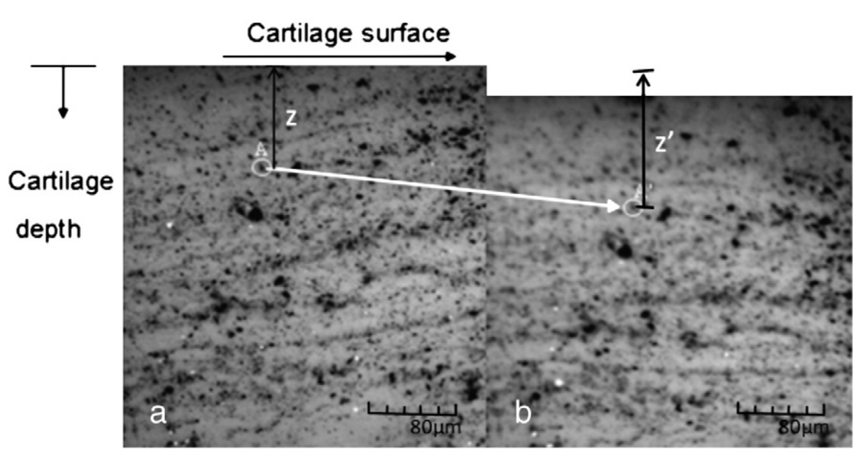

Fig. 2. Microscopic images of a section of articular cartilage before (a) and after loading (b).

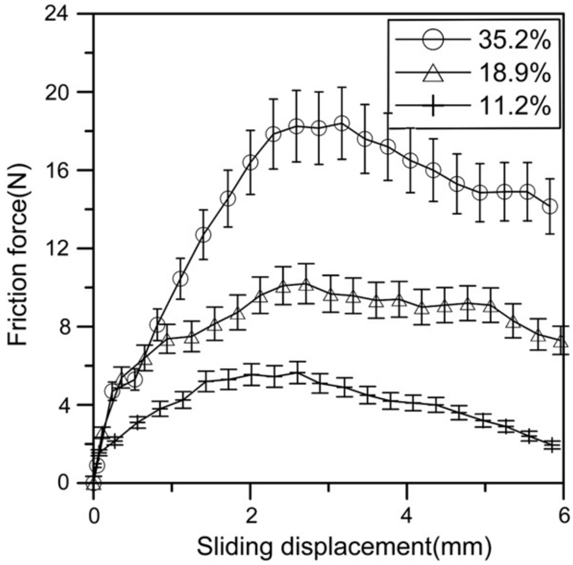

Fig. 3. Friction force–sliding displacement curves for cartilage with different compressive strain values at 0.33 mm/s.

rates and the friction forces at given sliding rate increase firstly and then decrease slowly with the slide of slider.

Fig. 7 shows the distributions of normal strain through cartilage depth at different sliding rates and with compressive strain of 18.9%. It is noted that the normal strain values through cartilage depth decrease slightly with increasing sliding rates. For the depth-dependent normal strains at different sliding rates the fitting curves by the expressions (2), (3), (4) and (5) agree with the experimental data very well.

4.4. Effect of sliding number on friction force and normal strain of articular cartilage

Fig. 8 shows the relation of friction force and sliding displacement for cartilage with different sliding numbers at sliding rate of 0.33 mm/s. It is shown that the first sliding friction forces are the largest and the friction forces decrease with increasing sliding numbers.

Fig. 9 shows the effect of sliding number on the normal strain of cartilage at sliding rate of 0.33 mm/s. It is found that the normal strain value increases with increasing sliding numbers and the increasing amplitude of normal strain between the first and second slide is significant.

5. Discussion

The results of many researchers [26–29] show that the friction coefficient of cartilage under constant load increases with sliding time, which means the friction force under constant load increases as the sliding time evolves. In this study the constant compressive strain is applied over the cartilage sample and the compressive force over the cartilage sample decreases as the sliding time evolves due to the viscoelastic characteristics of cartilage. Thus the friction forces of cartilage increase firstly due to the increase of friction coefficient and then decrease slowly due to the relaxation of compressive force with sliding time as shown in Fig. 3. The friction forces of the cartilage increase with increasing compressive strain (Fig. 3), which is in good agreement with the results of Naka et al. [30].

The friction force of cartilage depends not only on the compressive force but also on the sliding rate. The friction forces decrease slightly with increasing sliding rates as shown in Fig. 6. While the sliding rate increases from 0.33 to 1.67 mm/s, the maximum friction force decreases from 10.46 to 8.6 N. Articular cartilage has strain lag

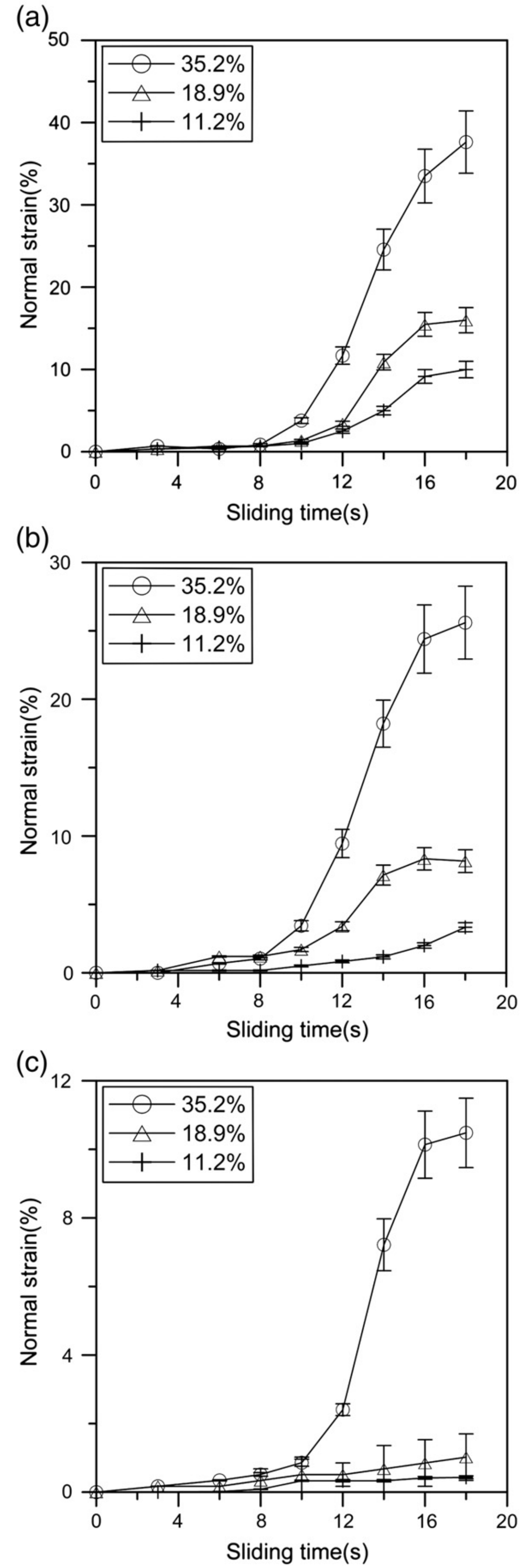

Fig. 4. Normal strain values of different layers for cartilage with sliding time with different compressive strain values and sliding rate of 0.33 mm/s. (a) superficial; (b) middle; (c) deep.

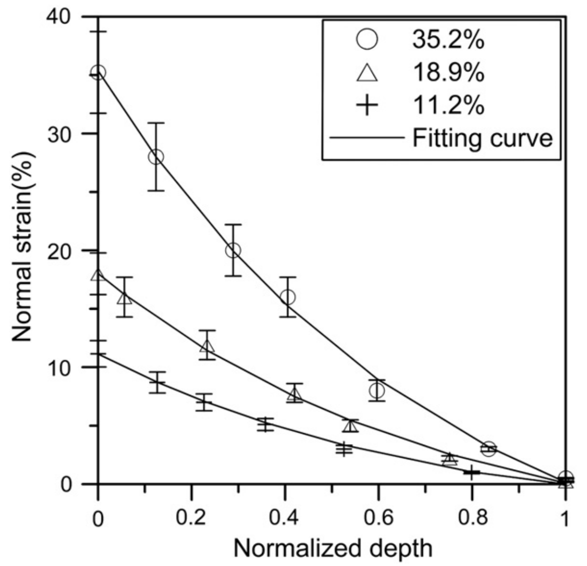

Fig. 5. Distributions of normal strain through cartilage depth with different compressive strain values at sliding rate of 0.33 mm/s.

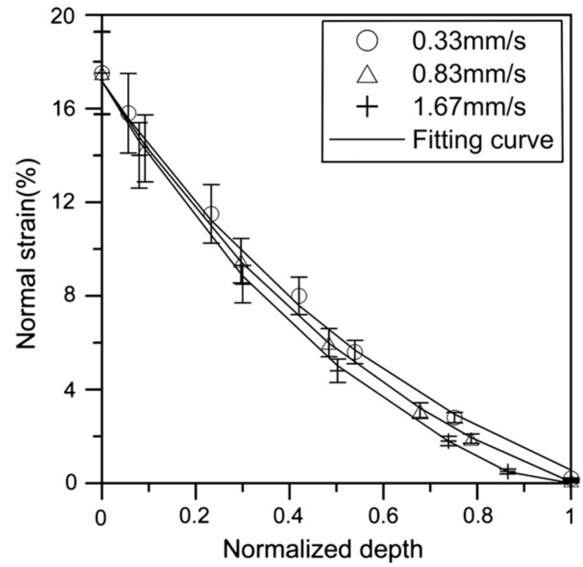

Fig. 7. Distributions of normal strain through cartilage depth at different sliding rates.

properties under stress due to its viscoelastic characteristics. Also, the friction force of the cartilage is larger when the cartilage deformed more because of the increased contact area between the friction counterparts. At high sliding rate, the contact area of the friction counterpart is smaller because the slider has passed the deformation region of the cartilage before the deformation region forms. Thus the deformation of cartilage is smaller and the friction force is smaller. Contrarily, as the deformation of cartilage is larger, so is the friction force of cartilage at low sliding rate. This result is in good agreement with the result of Pan et al. who investigated the friction properties of poly (viny1 alcohol) hydrogel as articular cartilage against titanium alloy [31].

The continuous sliding test under constant load was performed by Li et al. and it is found that the friction coefficient (or friction force) of cartilage-on-stainless steel contact increases gradually with increasing sliding numbers [9]. However the friction force of cartilage under constant compressive strain decreases with increasing sliding numbers in the present study. The reason is that the compressive force applied on the cartilage decreases due to its viscoelastic characteristics.

The mechanical properties of articular cartilage under physiological loads vary through the depth of cartilage. The depth-dependent strain, elastic modulus and Poisson's ratio of cartilage were investigated in unconfined compression [23–25,32]. However there is not any knowledge about the depth-dependent strain of cartilage under sliding load.

In this study, an optimized digital image correlation technique was applied to investigate the depth-dependent normal strain of articular cartilage under sliding load. This technique relies on the ability to reveal sufficiently random patterns on microscopy images of cartilage surfaces and the surface displacement and strain field can be obtained. The unconfined compression study [23,24] performed on cartilage specimens capitalizes on the usefulness of this methodology in characterizing two-dimensional strain fields. The depth-dependent normal strain distributions of cartilage under sliding load were obtained as shown in Figs. 4, 5 and 7. The normal strain values of different layers increase obviously with sliding time with compressive

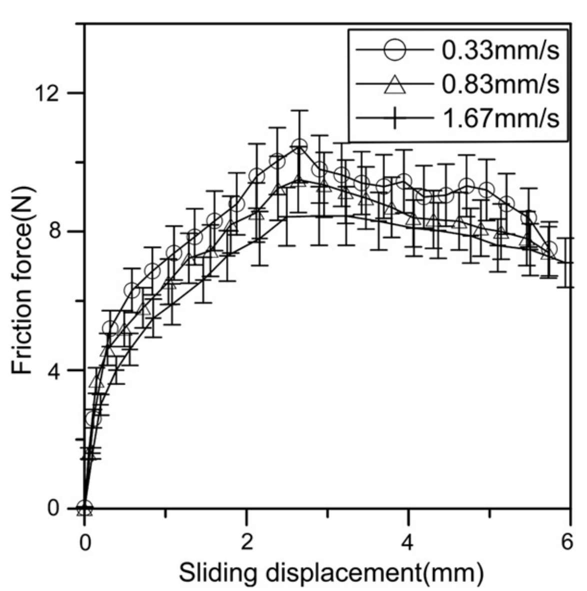

Fig. 6. Friction force–sliding displacement curves for cartilage at different sliding rates.

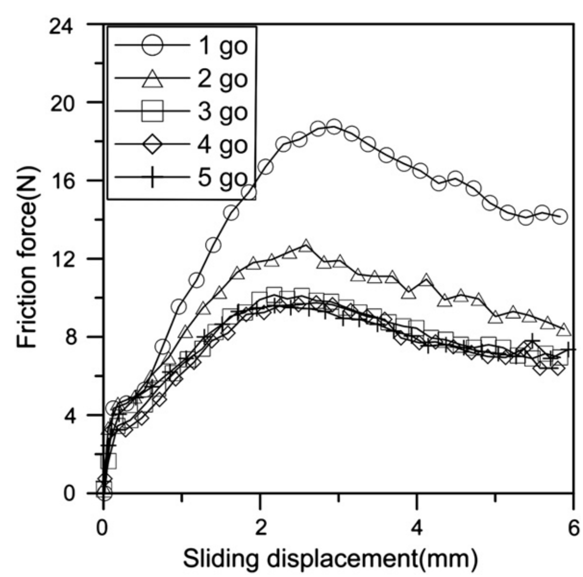

Fig. 8. Friction force–sliding displacement curves for cartilage with different sliding numbers.

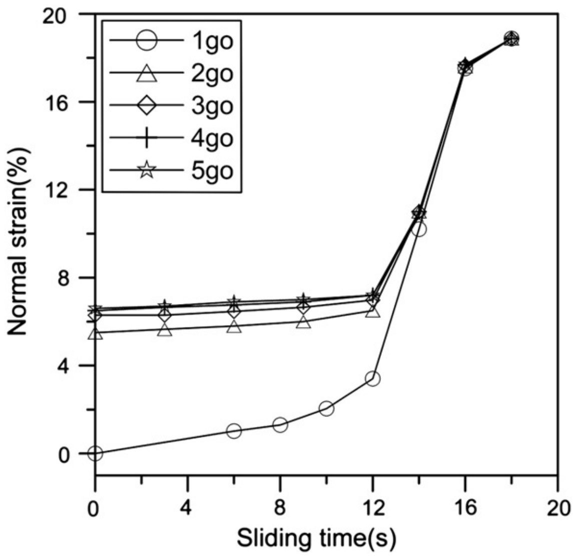

Fig. 9. Normal strain values of cartilage with sliding time with different sliding numbers.

strain of 35.2%. The normal strain values of superficial layer and middle layer appear in an increasing trend however little change of normal strain in deep layer is observed with sliding time with compressive strain of 18.9% and 11.2%. The normal strain value decreases along cartilage depth with constant compressive strain and the depth-dependent normal strain value increases with increasing compressive strain (Fig. 5), which agree with the results of Erne et al. and Gao et al. in unconfined compression [32,24]. The normal strain values through cartilage depth decrease slightly with increasing sliding rates because the contact time of cartilage and slider decreases at the larger sliding rate and moreover the deformation of cartilage reduces.

Naka et al. [28] proposed that it occurred for the exudation of the water in the cartilage when it underwent a sustained loading and the exudation of water when the cartilage was applied by sliding load was considered as the most important factor for the increase of the friction coefficient. Li et al. [9] found that the increasing amplitude of the friction coefficient for cartilage-on-stainless steel contact is larger during the initial sliding process by continuous sliding test. The results of Naka et al. and Li et al. indicate that a great deal of water in cartilage under sliding load outflows during the initial sliding process. This conclusion can be used to explain the results of the present study which the normal strain value increases with increasing sliding numbers and the increasing amplitude of normal strain during the former two sliding is significant (Fig. 9) due to the outflow of a great deal of water during the initial sliding process.

6. Conclusions

The optimized digital image correlation technique was applied to investigate the depth-dependent normal strain and friction force of articular cartilage under sliding load. The results show that the friction forces of cartilage increase firstly and then decrease slowly with the slide of slider and increase with increasing compressive strain values. The normal strain values of different layers increase obviously with sliding time with compressive strain of 35.2%. The normal strain values of superficial layer and middle layer appear the increasing trend and however little change of normal strain in deep layer is observed with sliding time with compressive strain of 18.9% and 11.2%. The depth-dependent normal strain values decrease along depth direction with constant compressive strain and the normal strain values of different normalized depth increase with increasing compressive strain. With increasing sliding rates the friction forces and depth-dependent normal strain values of cartilage decrease slightly. It is found that the first sliding friction force is the largest and then the friction force decreases with increasing sliding numbers. The normal strain value increases with increasing sliding numbers and the increasing amplitude of normal strain during the former two sliding is significant. The distributions of normal strain through cartilage depth considering the effects of compressive strain and sliding rate were fitted and the fitting curves agree with the experimental data with different compressive levels and sliding rates very well.

Acknowledgements

The project was partly supported by the National Natural Science Foundation of China (Nos. 31000422, 10872147 and 11172208) and China Postdoctoral Science Foundation (No. 20110490775).

References

[1] V.C. Mow, G.A. Ateshian, In: Basic Orthopaedic Biomechanics, Lippincott-Raven, Philadelphia, 1997, p. 273.
[2] E. Northwood, J. Fisher, Clin. Biomech. 22 (2007) 834.
[3] H. Forster, J. Fisher, P. I. Mech. Eng. 210 (1996) 109.
[4] C.J. Bell, E. Ingham, J. Fisher, J. Eng. Med. 220 (2006) 23.
[5] E. Northwood, J. Fisher, R. Kowalski, J. Eng. Med. 221 (2007) 263.
[6] R. Krishnan, M. Kopacz, G.A. Ateshian, J. Orthop. Res. 22 (2004) 565.
[7] J. Katta, S.S. Pawaskar, Z.M. Jin, E. Ingham, J. Fisher, J. Eng. Tribol. 221 (2007) 175.
[8] H. Forster, J. Fisher, J. Eng. Med. 213 (1999) 329.
[9] F. Li, Y.L. Su, J.P. Wang, G. Wu, C.T. Wang, J. Mater. Sci.: Mater. Med. 21 (2010) 147.
[10] M. Caligaris, G.A. Ateshian, Osteoarthr. Cartil. 16 (2008) 1220.
[11] S.S. Pawaskar, Z.M. Jin, J. Fisher, J. Eng. Tribol. 221 (2007) 165.
[12] R.K. Korhonen, M. Wong, J. Arokoski, R. Lindgren, H.J. Helminen, E.B. Hunziker, J.S. Jurvelin, Med. Eng. Phys. 24 (2002) 99.
[13] A. Thambyah, N. Broom, J. Anat. 209 (2006) 611.
[14] J.P. Arokoski, M.M. Hyttinen, T. Lapvetelainen, P. Takacs, B. Kosztaczky, L. Modis, V. Kovanen, H. Helminen, Ann. Rheum. Dis. 55 (1996) 253.
[15] W. Wilson, C.C. van Donkelaar, B. van Rietbergen, R. Huiskes, J. Biomech. 38 (2005) 1195.
[16] P. Julkunen, W. Wilson, J.S. Jurvelin, J. Rieppo, C.J. Qu, M.J. Lammi, R.K. Korhonen, J. Biomech. 41 (2008) 1978.
[17] R.K. Korhonen, W. Herzog, J. Biomech. 41 (2008) 480.
[18] X. Bi, X. Yang, M.P. Bostrom, N.P. Camacho, Biochim. Biophys. Acta 1758 (2006) 934.
[19] X. Bi, X. Yang, M.P. Bostrom, D. Bartusik, S. Ramaswamy, K.W. Fishbein, R.G. Spencer, N.P. Camacho, Anal. Bioanal. Chem. 387 (2007) 1601.
[20] N.P. Camacho, P. West, P.A. Torzilli, R. Mendelsohn, Biopolymers 62 (2001) 1.
[21] K. Potter, L.H. Kidder, I.W. Levin, E.N. Lewis, R.G. Spencer, Arthritis Rheum. 44 (2001) 846.
[22] J. Rieppo, M.M. Hyttinen, R. Lappalainen, J.S. Jurvelin, H.J. Helminen, Trans. Orthop. Res Soc. 29 (2004) 1021.
[23] C.C.B. Wang, J.M. Deng, G.A. Ateshian, C.T. Hung, J. Biomech. Eng. 124 (2002) 557.
[24] L.L. Gao, C.Q. Zhang, L.M. Dong, Y.W. Jia, Mater. Sci. Eng. C 32 (2012) 119.
[25] N. Sakai, Y. Hagihara, T. Furusawa, N. Hosoda, Y. Sawae, T. Murakami, Tribol. Int. 46 (2012) 225.
[26] K. Mabuchi, H. Fujie, Clin. Biomech. 11 (1996) 121.
[27] J.E. Pickard, J. Fisher, E. Ingham, J. Egan, Biomaterials 19 (1998) 1807.
[28] M.H. Naka, K. Hattori, K. Ikeuchi, J. Biomech. 39 (2006) 2164.
[29] R. Krishnana, E.N. Marinerb, G.A. Ateshian, J. Biomech. 38 (2005) 1665.
[30] J. Katta, Z.M. Jin, E. Ingham, J. Fisher, Med. Eng. Phys. 30 (2008) 1349.
[31] Y.S. Pan, D.S. Xiong, R.Y. Ma, Wear 262 (2007) 1021.
[32] O.K. Ernea, J.B. Reidb, L.W. Ehmkea, M.B. Sommersa, S.M. Madeya, M. Bottlanga, J. Biomech. 38 (2005) 667.